Pendulum Beams: A Window into the Quantum Pendulum

Enrique J. Galvez[a], Fabio J. Auccapuclla[a,b], Kristina L. Wittler[a], and Yingsi Qin[a]

[a]Department of Physics and Astronomy, Colgate University, Hamilton, New York 13346, U.S.A.
[b]Departamento de Ciencias, Sección Física, Pontificia Universidad Católica del Perú, Lima, Apartado 1761, Perú

ABSTRACT

Parallels between the Helmholtz and Schrödinger equations can be exploited for using light beams to investigate quantum problems. We present the study of a type of non-diffracting beams known as pendulum beams, where the optical modes satisfy a form of the Helmholtz equation that is identical to the Schrödinger equation for the mechanical pendulum. We prepared optical beams in the corresponding eigenmodes and made measurements of their Fourier spectrum. We find remarkable quantitative agreement between the measured angular spectrum and the quantum mechanical probabilities.

Keywords: Non-diffracting beams, Pendulum beams, Mathieu beams, Quantum pendulum

1. INTRODUCTION

Optical beams are described classically by the Helmholtz wave equation. It has long been known that this equation can be put in the same form as the Schrödinger equation.[1] It gives interesting parallels between light and quantum phenomena. In this work we exploit one such parallel. It involves the problem of the quantum solution of the simple mechanical pendulum. For small angles the pendulum equation of motion reduces to the harmonic oscillator, one of the most studied mechanical problems in physics. For pendulum oscillations at large angles it is a rich nonlinear problem,[2] extending to the non-linear rotor for large energies. The quantum mechanical solution of this problem has been presented numerous times before.[3–7] It is expressed in terms of the Mathieu equation. Non-diffracting optical beams that are solutions to the Helmholtz equation in elliptical coordinates satisfy the Mathieu equation, and so are called Mathieu beams.[8,9] These beams give rise to helical-elliptical solutions that contain an interesting arrays of optical vortices.[9,10]

Previous demonstrations investigated the types of Mathieu beams that can be produced.[8–12] Non-helical Mathieu beams are solutions with a direct correspondence to the quantum pendulum eigenstates.[13] In this work we compare measurements of pendulum beams to the quantum probabilities of the pendulum solutions.

2. THEORY

2.1 Quantum Pendulum

We consider a pendulum bob defined in Fig. 1(a): a bob of mass m connected to a pivot point through a rigid massless rod of length l. It swings under the influence of gravity with constant g. The Schrödinger equation for the problem is given by

$$-\frac{\hbar^2}{2ml^2}\frac{d^2\psi}{d\theta^2}+V\psi=E\psi \tag{1}$$

where the potential is, following Fig. 1(a), given by

$$V=mgl(1-\cos\theta) \tag{2}$$

Further author information: E.J.G.: E-mail: egalvez@colgate.edu (Send correspondence to E.J.G.)
E.J.G.: E-mail: egalvez@colgate.edu, Telephone: 1 315 228-7205
Proc. SPIE **10935**, 1093509 2019.

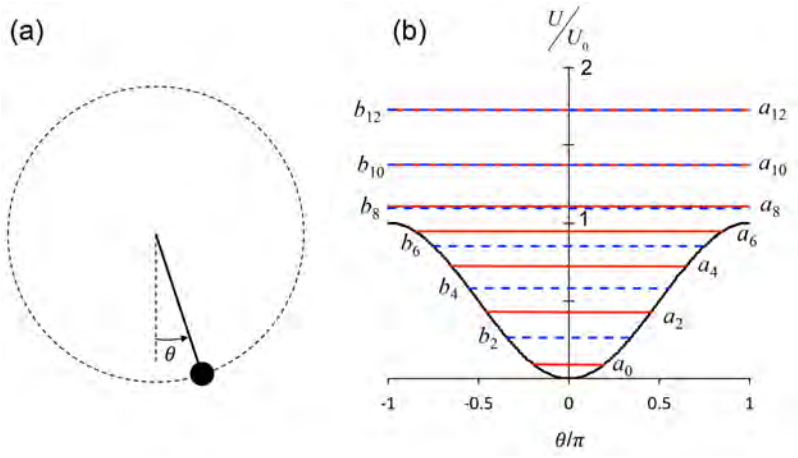

Figure 1. (a) Set up for the mechanical pendulum. (b) Graph of the potential energy well and the lowest energy levels for the case when the barrier height is $q = 30$. Solid and dashed lines correspond to the even and odd solutions respectively.

Following Baker[7] we use the substitutions for the energy scaled by $E_0 = \hbar^2/2ml^2$.

$$U_0 = \frac{mgl}{E_0} \tag{3}$$

and

$$\varepsilon = \frac{E}{E_0} \tag{4}$$

If we let m be the mass of the electron and l the atomic radius, this scaling unit is the familiar Bohr energy, $E_0 = 13.6$ eV. However, the energy constant of the pendulum is small due to the weakness of gravity. If we proceed with the pendulum bob being the electron an atomic radius away from the pivot point, we get $U_0 = 2.1 \cdot 10^{-22}$ eV. Thus, there are no realistic mechanical test cases to investigate. Following these substitutions, the equation becomes

$$-\frac{d^2\psi}{d\theta^2} + U_0(1 - \cos\theta)\psi = \epsilon\psi. \tag{5}$$

We now do the substitution

$$\theta = 2\chi \tag{6}$$

and Eq. 1 becomes of the same form as the Mathieu equation:[14]

$$\frac{d^2\psi}{d\chi^2} + (a - 2q\cos 2\chi)\psi = 0, \tag{7}$$

where a is a separation constant, which in the solution gives rise to the quantum numbers a_i and b_i for even and odd eigenfunctions, respectively. The energy of the pendulum is related to a by

$$\varepsilon = \frac{a}{4} + U_0 \tag{8}$$

and

$$\varepsilon_b = q = 2U_0 \tag{9}$$

is the height of the barrier of the cosine-shaped potential well, as seen in Fig. 1(b). The parameter q depends on g, allowing us to investigate various scenarios of the quantum pendulum. The energy solutions of the quantum pendulum are well known.[7,14] Figure 2 shows the energy as a function of q. By manipulating q we can select how many bound levels we may have. When $\varepsilon < \varepsilon_b$ the classical pendulum swings anharmonically. It resembles the harmonic oscillator for small angles of the maximum elongation θ_M.

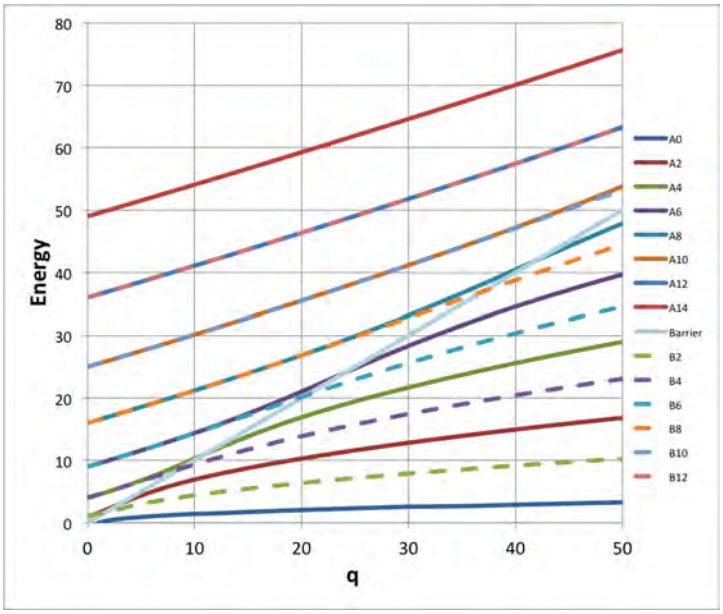

Figure 2. Energy eigenvalues for the lowest states of the quantum pendulum as a function of the barrier height q. Solid and dashed lines are the even and odd solutions, respectively. We also show the energy of the potential barrier.

The oscillatory regime is when $E < 2mgl$. The period of the motion for this case is given by

$$\tau_{\rm osc} = 4\sqrt{\frac{l}{2g}}\int_0^{\theta_M} \frac{d\theta}{\sqrt{\cos\theta - \cos\theta_M)}}. \tag{10}$$

This solution becomes an elliptic integral that can be solved either approximately or numerically. The period reduces to $\tau = 2\pi\sqrt{l/g}$ in the limit of small oscillations. When $E > 2mgl$ the pendulum becomes a rotor. Its period is given by

$$\tau_{\rm rot} = 2l\sqrt{\frac{m}{2}}\int_0^{\pi} \frac{d\theta}{\sqrt{E - mgl(1 - cos\theta)}}. \tag{11}$$

This result reduces to $\tau = 2\pi\sqrt{ml^2/E}$ in when $E \gg mgl$. When E is just above q in the rotor solutions, the rotor describes a nonlinear rotation spending more time at $\theta = \pi$ than at $\theta = 0$. Thus, a good indicator of the motion is the ratio of the instantaneous angular frequencies at those two extrema:

$$\frac{\omega(\pi)}{\omega(0)} = \sqrt{1 - \frac{q}{E}}. \tag{12}$$

The solutions to the quantum pendulum have to satisfy $\psi(\theta) = \psi(\theta + 2\pi)$ or $\psi(\chi) = \psi(\chi + \pi)$, which restricts the solutions to even index. There are two types of solutions to the angular Mathieu equation (7) depending on the parity about $\chi = 0$:

$$\psi = \begin{cases} \mathrm{ce}_n = \sum_{k=0}^{\infty} A_k \cos(k\chi) & k \text{ even}, n = 0, 2, 4, \ldots \\ \mathrm{se}_n = \sum_{k=2}^{\infty} B_k \sin(k\chi) & k \text{ even}, n = 2, 4, 6, \ldots \end{cases} \tag{13}$$

with ce and se being the cosine-elliptical and sine-elliptical Mathieu functions, and A_k and B_k are coefficient that result from the solution.[14] For these solutions of the Mathieu equation involving even indices n the period of the functions in the variable χ is π. This is consistent with the period of the real pendulum to be that of the physical coordinate θ: 2π. Both functions have even parity about $\chi = \pi/2$, whereas about $\chi = 0$ the cosine elliptical is even and the sine elliptical is odd. For $q \to 0$ (zero gravity, free rotor case), the solutions are of

the form $\cos n\chi$ and $\sin n\chi$. Moreover, the functions can be recognized by the number of zero-crossings in the interval $\chi \in [0, \pi]$: n for cosine and $n+1$ for sine.

Figure 3 shows graphs of the probability of finding the bob at a given angle when $q = 30$. The top row corresponds to the cosine-elliptical wavefunctions and the bottom row to the sine-elliptical wavefunctions. We list the quantum number n for each case. Below it we also list the energy of the state E relative to the barrier height q. For the oscillatory solutions a relevant parameter that lets us visualize the relation to the classical case via the angle of maximum elongation (turning point) θ_M. For the rotor-like solutions we list the ratio of the instantaneous maximum and minimum angular frequencies in the rotation.

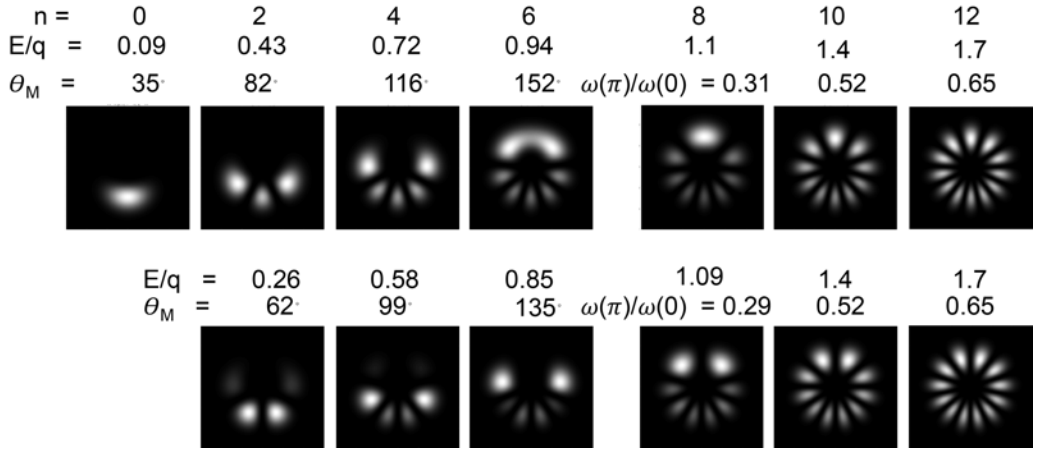

Figure 3. Computed probabilities for finding the quantum pendulum bob as a function of the angle θ for $q = 30$. The top and bottom rows correspond to the even and odd eigenfunctions, respectively. We also list the quantum number n and the pendulum energy eigenvalue relative to the barrier height ε/q. For oscillatory solutions $\varepsilon/q < 1$ we also list the classical turning angle θ_M, and for the rotor solutions $\varepsilon/q > 1$ we list the ratio of the angular frequencies for $\theta = \pi$ and $\theta = 0$.

2.2 Pendulum Beams

Light beams satisfy the Helmholtz equation. One type of solution, known as non-diffracting involves an intensity that does not depend on the z-coordinate, leading to the 2-dimensional Helmholtz equation:

$$\frac{\partial^2 U}{\partial x^2} + \frac{\partial^2 U}{\partial y^2} + k_t^2 U = 0. \tag{14}$$

where k_t is the propagation constant in the transverse plane. We now express the 2-dimensional Helmholtz equation in elliptical coordinates:

$$\begin{cases} x = e \cosh\xi \cos\chi \\ y = e \sinh\xi \sin\chi, \end{cases} \tag{15}$$

where the coordinates of each point are the intersections of hyperbolas specified by χ and ellipses specified by ξ. e is a parameter that specifies the distance from each foci to the origin (i.e., $x = \pm e$ is the location of the foci). The variable ξ specifies the ellipticity of the ellipse by

$$\epsilon = \tanh\xi. \tag{16}$$

Separation of variables results in two equations in terms of the radial-like variable ξ and the angular-like variable χ. The radial and angular equations are

$$\frac{d^2 R}{d\xi^2} - (a - 2q\cosh 2\xi)R = 0 \tag{17}$$

$$\frac{d^2 \Psi}{d\chi^2} + (a - 2q\cos 2\chi)\Psi = 0 \tag{18}$$

where a is a constant and

$$q = \frac{e^2 k_t^2}{4}. \tag{19}$$

The angular equation has the exact form of the Mathieu equation (Eq. 7), with angular-like solutions given by Eqs. 13. The radial-like solution is expressed in terms of the radial Mathieu functions, which are elliptical Bessel-like oscillatory functions of ξ,[14]

$$R(\xi; q) = \begin{cases} \mathrm{Je}_n(\xi; q) \text{ and } \mathrm{Jo}_n(\xi; q) & \text{first kind} \\ \mathrm{Ne}_n(\xi; q) \text{ and } \mathrm{No}_n(\xi; q) & \text{second kind} \end{cases} \tag{20}$$

where "e" and "o" stand for even and odd parity, respectively. The pendulum beam then has a wavefunction of the form

$$U(\xi, \chi; q) = \begin{cases} \mathrm{ce}_n(\chi; q)\mathrm{Je}_n(\xi; q) \\ \mathrm{se}_n(\chi; q)\mathrm{Jo}_n(\xi; q) \end{cases} \tag{21}$$

The Fourier transform of the solutions has the form[13]

$$\mathrm{FT}[U(\xi, \chi; q)] = \begin{cases} \mathrm{ce}_n(\theta/2; q)\delta(k - k_t) \\ \mathrm{se}_n(\theta/2; q)\delta(k - k_t), \end{cases} \tag{22}$$

where δ is the Dirac delta function. The Fourier transform is then a ring modulated by the angular solution of the Mathieu equation, which is expressed as a function of half the angle of the pendulum in real space. As we will see below, this has an important bearing in the experimental measurements. The even and odd solutions and their Fourier transforms for $n = 4$ and $q = 30$ are shown in Fig. 4.

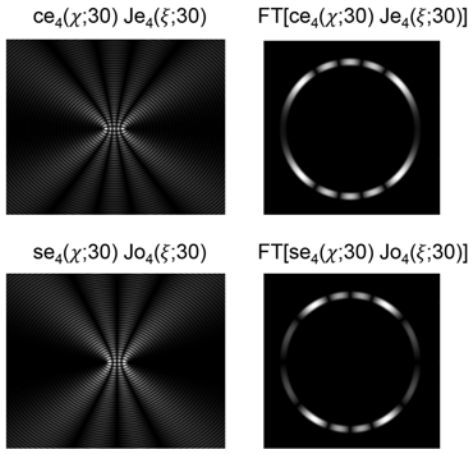

Figure 4. Predicted intensities for even (top) and odd (bottom) pendulum wavefunctions (left) and Fourier transforms (right), corresponding to the case $n = 4$ $q = 30$.

3. MEASUREMENTS

3.1 Methods

We produced pendulum beams by phase encoding a nearly flat-top beam from a HeNe laser using a spatial light modulator. A schematic of the apparatus is shown in the Fig. 5. The light from a helium-neon laser (HeNe) was expanded, spatially filtered and cropped by an iris. It was incident on a spatial light modulator (SLM) that encoded the appropriate phase pattern onto the beam upon reflection. The encoded pattern contained the azimuthal and radial phase of the pendulum beam on top of a linear phase blaze so that the beam appeared on

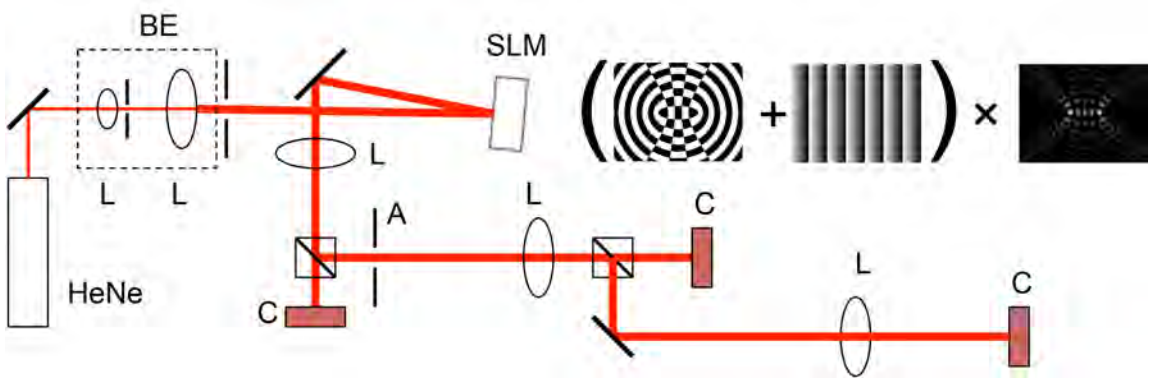

Figure 5. Schematic of the apparatus used for the experiments. Light from a HeNe laser travels through a $\times 5$ Newtonian beam expander. The mode is encoded by an SLM and it is re-imaged by 3 lenses (L) of focal length f so that the beam and its Fourier transforms (masked and unmasked) were captured by digital cameras (C). The Fourier transform was spatially filtered by an aperture mask (A). The distances between lenses is $2f$ and the distances between lenses and cameras was f. The insert shows the pattern encoded onto the SLM for the case $n = 4$ and $q = 30$ with even parity.

diffraction. The depth of the phase pattern was further modulated by the amplitude of the mode, which reduces the diffraction efficiency around the zeros of the desired mode. This approach is shown pictorially by the insert in Fig. 5.

A part of the beam was diverted to a camera to image the raw Fourier transform of the beam. This was done at the focal plane of the first lens after the SLM. The lens was located a focal length away from the SLM ($\sim$ 29 nm). The other portion of the beam was spatially filtered at the Fourier plane with an aperture (A). A second lens located a focal length away from the aperture. The pendulum pattern, a non-diffracting beam, assembled between f and $2f$ away from the second lens. A portion of the light heading to the camera imaging the pendulum mode was diverted by a beam splitter. It passed through a lens a focal length away, followed by a camera a focal length further. This way, the last camera recorded the Fourier transform of the imaged beam.

3.2 Results

Figure 6 shows a sample of the data that we recorded. Three of the columns show the pendulum modes corresponding to the even eigenfunctions of the oscillating pendulum ($n = 0, 4, 6$). The last column shows the pendulum mode corresponding to the odd eigenfunction of the rotating pendulum ($n = 10$). All of these modes were obtained for the case featured in this article: $q = 30$. The first row (a) shows the computed beam modes, whereas the second row (b) shows the measured beam modes. As can be seen, the measurements and the computations are in excellent qualitative agreement. We also verified the non-diffracting character of the beams by taking images at various distances within the range that defines the overlap of rays.

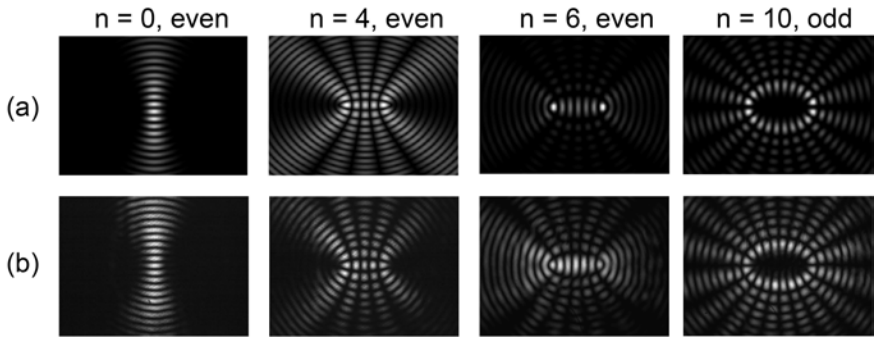

Figure 6. Computed (a) and measured (b) pendulum modes for several pendulum states with $q = 30$.

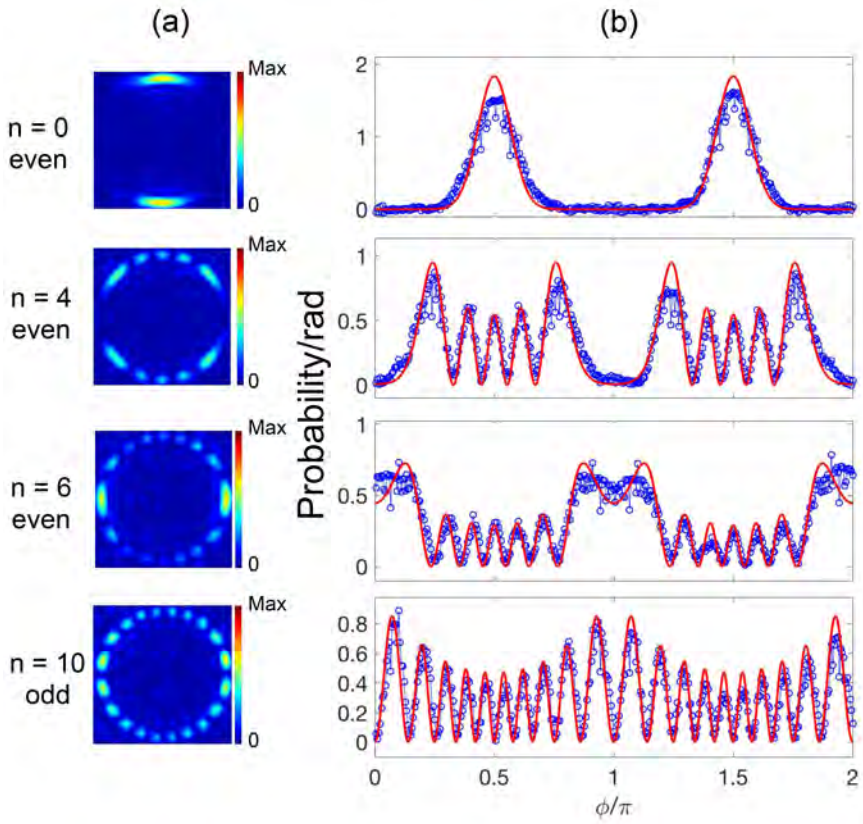

Figure 7. (a) Images of the light at the Fourier-transform plane. (b) Graph of the data (symbols) obtained by integrating the light patterns in (a) over discrete intervals along a ring; with the calculated quantum mechanical probabilities (solid line). This is done for the same 4 cases as in Fig. 6.

We did a more quantitative comparison between measurements and the predictions of the quantum pendulum. Since the light pattern obtained at the Fourier Transform plane is proportional to the quantum-mechanical probabilities (i.e., the square of the functions shown in Eq. 22), we integrated the light recorded in the images in the Fourier-transform plane (Fig. 7(a)) along a ring over angular intervals. We tried several angular increments and values of inner and outer ring radii. We then normalized the data, after subtracting the background counts, and compared it to the quantum-mechanical probability. Figure 7(b) shows the comparisons for the four cases of Fig. 6. Because the angular coordinate of the pendulum is twice the beam's angular coordinate, the beam's Fourier transform is a 2-1 mapping of the pendulum angle, and so the probability for $\theta \exists [0, 2\pi]$ appears in the top half of the image in Fig. 6(c) for the angular range $[\pi/2, 3\pi/2]$ and is repeated in the bottom half of the image for the angular range $[3\pi/2, 5\pi]$.

We find that the agreement between measurements and theoretical calculations is remarkably close, especially given that there were not adjustable parameters other than subtracting the background counts. The comparison reflects the well known connections between optical beams and their optical Fourier transforms,[15] yet it is interesting that the comparison extends so well into complex light beams. This comparison could be improved with the use of annular-ring type of apertures in the Fourier plane.[12,16]

4. DISCUSSION AND CONCLUSIONS

In summary, we present a study of pendulum beams to simulate the quantum pendulum. By varying the beam parameters n and q we are able to access particular situations of the pendulum: a certain potential energy barrier height and a particular quantum state. When the energy of the state is below the barrier, the full solutions are

of the oscillating anharmonic pendulum, and when the energy is above the barrier, the solutions correspond to the anharmonic rotor. From the experimental light beams we are able to extract data that compares remarkably well with the quantum mechanical probabilities of the quantum pendulum.

ACKNOWLEDGMENTS

We would like to thank M.R. Dennis for introducing us to this problem and to S. Chávez-Cerda for useful discussions. This work was funded by the grant from the National Science Foundation PHY-1506321.

REFERENCES

[1] Marte, M. and Stenholm, S., "Paraxial light and atom optics: The optical Schrödinger equation and beyond," *Phys. Rev. A* **56**, 2940–2953 (1997).

[2] Strogatz, S., [*Nonlinear Dynamics and Chaos: With Applicaitons to Physics, Biology Chemistry and Engineering*], Perseus Books (1994).

[3] Condon, E., "The physical pendulum in quantum mechanics," *Phys. Rev.* **31**, 891–894 (1928).

[4] Pradhan, T. and Khare, A., "Plane pendulum in quantum mechanics," *Am. J. Phys.* **41**, 59–66 (1973).

[5] Aldrovandi, R. and Ferreira, P. L., "Quantum pendulum," *Am. J. Phys* **48**, 660–664 (1980).

[6] Cook, G. and Zaidins, C., "The quantum point-mass pendulum," *Am. J. Phys.* **54**, 259–267 (1986).

[7] Baker, G., Blackburn, J., and Smith, H., "The quantum pendulum: Small and large," *Am. J. Phys.* **70**, 525–531 (2002).

[8] Gutiérrez-Vega, J., Iturbe-Castillo, M., and Chávez-Cerda, S., "Alternative formulation for invariant optical fields: Mathieu beams," *Opt. Lett.* **25**, 1493–1495 (2000).

[9] Gutiérrez-Vega, J., Iturbe-Castillo, M., Ramírez, G., Tepichín, E., Rodríguez-Dagnino, R., Chávez-Cerda, S., and New, G., "Experimental demonstration of Mathieu beams," *Opt. Commun.* **195**, 35–40 (2001).

[10] Chávez-Cerda, S., Gutiérrez-Vega, J., and New, G., "Elliptic vortices of electromagnetic waves," *Opt. Lett.* **26**, 1803–1805 (2001).

[11] Chávez-Cerda, S., Padgett, M., Allison, I., New, G., Gutiérrez-Vega, J., O'Neil, A., MacVicar, I., and Courtial, J., "Holographic generation and orbital angular momentum of high-order Mathieu beams," *J. Opt. B* **4**, S52–S57 (2002).

[12] Hernández-Hernández, R., Teborg, R., Ricardez-Vargas, I., and Volke-Sepúlveda, K., "Experimental generation of Mathieu–Gauss beams with a phase-only spatial light modulator," *Appl. Opt.* **49**, 6903–6909 (2010).

[13] Dennis, M. and Ring, J., "Propagation-invariant beams with quantum pendulum spectra: from Bessel beams to Gaussian beam-beams," *Opt. Lett.* **38**, 3325–3328 (2013).

[14] Gutiérrez-Vega, J., Rodríguez-Dagnino, R., Meneses-Nava, M., and Chávez-Cerda, S., "Mathieu functions, a visual approach," *Am. J. Phys.* **71**, 233–242 (2003).

[15] Goodman, J., [*Introduction to Fourier Optics*], McGraw-Hill (1996).

[16] Arrizón, V., de-la Llave, D. S., Ruiz, U., and Méndez, G., "Efficient generation of an arbitrary nondiffracting Bessel beam employing its phase modulation," *Opt. Lett.* **34**, 1456–1458 (2009).